Solar light-driven reduction of crystal violet by a composite of g-C_3N_4, β-Ag_2Se, γ-Fe_2O_3 and graphite

Roberto C. Dante [a*], Pablo Martín-Ramos [b], Pedro Chamorro-Posada [c], Dario Rutto [d], José Vázquez-Cabo[e], Denisse G. Dante [a], Riccardo Barberis [d], Óscar Rubiños-López [e]

[a] R&D Department, 2Dto3D S.r.l.s. Via Revalanca 5, San Firmino, Revello (CN) 12036, Italy.
[b] EPS, Instituto de Investigación en Ciencias Ambientales (IUCA), Universidad de Zaragoza, Carretera de Cuarte s/n, 22071, Huesca, Spain
[c] Dpto. de Teoría de la Señal y Comunicaciones e IT, Universidad de Valladolid, ETSI Telecomunicación, Paseo Belén 15, 47011 Valladolid, Spain.
[d] R&D Department, Burgo Group S.p.A., Via Roma 10, 12039 Verzuolo (CN), Italy
[e] Dpto. de Teoría de la Señal y Comunicaciones, Universidad de Vigo, ETSI Telecomunicación, Lagoas Marcosende s/n, Vigo, Spain.
[*]Corresponding author: E-mail: rcdante@2dto3dmaterials.com

Abstract. In this work, a new g-C_3N_4-based Z-scheme with γ-Fe_2O_3 and β-Ag_2Se both n-type semiconductors, and graphite to favor electron exchange is presented. The composite material (AgFeCN) was studied by XRD, FTIR, UV-Vis, TEM, XPS, TGA, DSC and TOF-SIMS, and the ability of this photocatalytic system to act as a photo-reductant was assessed using crystal violet (CV^+) dye. Solar light driven photo-reduction of CV^+ in the presence of tri-sodium citrate evidenced a synergistic enhancement of the activity of the composite towards reduction, with ~20 times higher conversion rates per unit of surface area than those of g-C_3N_4. Photo-oxidation experiments under Xe lamp irradiation in the presence of H_2O_2 also showed that the AgFeCN composite featured a higher activity (~8×) than g-C_3N_4. This Z-scheme may deserve further study as a photo-reductant to obtain hydrogen or hydrogenated compounds. Moreover, the use of CV^+ represents a facile procedure that can aid in the selection of new photocatalysts to be used in hydrogen production.

Keywords: photocatalysis, carbon nitride, dye, semiconductors, Z-scheme

INTRODUCTION

Graphitic carbon nitride (g-C_3N_4) is a supramolecular polymeric material, held together by diffuse hydrogen bonds, which generally features a low degree of crystallinity. It was first synthesized by Berzelius and Liebig in 1834 [1]. Pauling and Sturdivant then clarified that this substance contained a C_6N_7 nucleus ("cyameluric nucleus"), which is currently referred to as either heptazine or tri-*s*-triazine nucleus [2]. Nowadays there is a widespread agreement on the structure of the material, regarded as a polymer with a $C_6N_7(NH_2)NH$ repeating unit. From a morphological point of view, it tends to form corrugated lamellae, which can result in the formation of globular and even tubular particles, depending on synthesis conditions (e.g., maximum temperature and treatment time) [3]. In terms of its electronic properties, g-C_3N_4 exhibits characteristics of a wide-bandgap semiconductor, with low mobility of charges.

Due to its heptazine repeating units, this material has both Lewis and Brønsted sites, and "cages" that can coordinate metals and form stable complexes. The presence of these sites makes polymeric carbon nitride a very versatile material, which combines characteristics of polymers, catalysts and semiconductors. Hence, its reported applications are very wide, ranging from electronics and optoelectronics to

photocatalysis (including specific organic reactions, such as oxidative addition to aromatic rings [4]), hydrogen generation [5], gases [6] and glucose [7] sensing, or photovoltaics [8], to name a few.

The determining factor in the use of g-C_3N_4 as an effective photocatalyst is charge separation (exciton dissociation), as well as the exciton binding energy. Indeed, considering that in g-C_3N_4 one is dealing with Frenkel excitons, the balance between stability and separation of exciton charges seems to be one of the key factors to achieve a high yield in hydrogen production. Recombination of charges represents a loss of efficiency in the whole photonic process, and mechanisms and methods that allow to increase exciton lifetime are welcome. Moreover, the absorbed photons are mostly in the UV range due to the bandgap of carbon nitride materials (of around 3 eV, corresponding to 413 nm, at the edge between UV and visible radiation). The strategy of lowering the bandgap to increase photon absorption can decrease the overall catalyst efficiency due to the many overpotentials involved in the photocatalysis process. On the other hand, coupling g-C_3N_4 with semiconductors with lower bandgaps (that allow to absorb more photons) can enable the Z-scheme, which, in this case, consists in electron "feeding" from a semiconductor that harvests photons from visible light to the valence band of g-C_3N_4 [9]. Both pathways exploit the versatile nature of polymeric g-C_3N_4 to be doped, to coordinate molecules and to wrap nanoparticles.

Among the semiconductors that g-C_3N_4 can be coupled to, iron and silver-based materials has been reported to increase either the electrochemical performance (exhibiting a remarkable efficiency toward oxygen reduction processes in an alkaline environment [10]) or the catalytic properties of carbon nitride [11].

In this study presented herein, with a view to increasing the redox power of g-C_3N_4, an Ag_2Se-Fe_2O_3-graphite-g-C_3N_4 (AgFeCN) composite was prepared, and its photocatalytic performance was compared with that of pristine g-C_3N_4. According to the Z-scheme scheme shown in Figure 1, Ag and Fe compounds would support the electron "feeding" process (although Ag_2Se is a n-type narrow-band semiconductor, β-Ag_2Se nanoparticles exhibit an optical bandgap of around 2 eV [12,13], and Fe(III) oxide also is a n-type semiconductor with a bandgap of around 2 eV [14]), while graphite would favor electron exchange, improving the overall efficiency [15].

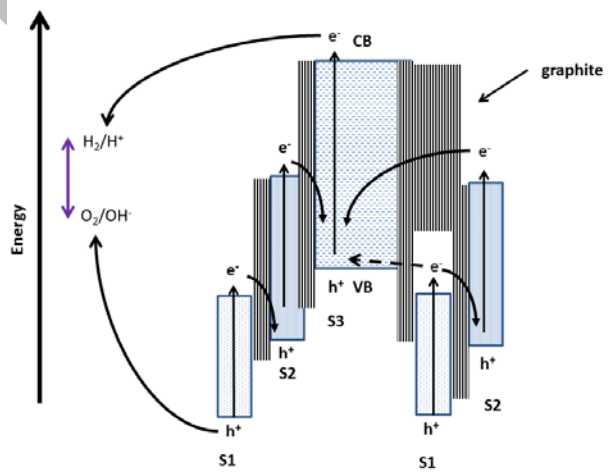

Figure 1. Possible double Z-scheme for water splitting in the studied composite, which consists of β-Ag_2Se (S1), γ-Fe_2O_3 (S2), g-C_3N_4 (S3) and graphite. The scheme is based on the application of the well-known formula used to determine the energy of the valence band (E_{VB}), and consequently that of the conduction band: $E_{VB} = \chi - E^e + 0.5E_g$, where χ, E^e, and E_g are the absolute electronegativity (determined as the geometric mean between elemental

electronegativities), the energy of free electrons on the hydrogen scale (4.5 eV), and the bandgap energy of the semiconductor, respectively [16,17].

For the photocatalytic redox tests, crystal violet (CV^+) dye was chosen. This dye is violet colored in its oxidized form and colorless in its reduced form, leuco crystal violet (LCV). Given that its reduction potential is -1.0 eV [18], very close to that of hydrogen, it may be put forward a possible model system to select new photocatalysts through simple spectrophotometric UV-Vis studies. By studying the reduction reaction of CV^+ to LCV, potential photocatalysts more inclined to reduction (involving hydrogen exchange) than to oxidation may be identified in a facile manner.

EXPERIMENTAL

Materials and synthesis procedure

Melamine cyanurate (MCA) (CAS No. 37640-57-6; supplied by Nachmann S.r.l., >99.0%) precursor was mixed with SeO_2 (CAS No. 7446-08-4; Sigma Aldrich, >99.9%) in a 3:1 molar ratio (69 g of MCA were mixed with 10 g of SeO_2 in 0.8 L of water) in a beaker, and was sonicated for 50 min at room temperature, leading to a suspension with pH 1.5. This suspension was allowed to stand for 12 h, and then was dried in a vacuum oven at 200 °C for 6 h (the precursor is deliquescent and hygroscopic). Samples of the dry solid (slightly reddish) were ground in an agate mortar and were placed in a sealed Vycor® glass vial with a valve. 0.254 g of $AgNO_3$ (CAS No. 7761-88-8; Sigma-Aldrich, ≥99.0%), 1.009 g of $FeSO_4 \cdot 7H_2O$ (CAS No. 7782-63-0; Sigma-Aldrich, ≥99%) and 0.510 g of natural flake graphite (supplied by Asbury Carbons, grade micro 850) were mixed with 32.808 g of a MCA previously mixed with SeO_2 as described. The final yield after a treatment in an oven in air at 600 °C for 30 min was 27.6 wt%. Pristine g-C_3N_4, used as a reference, was prepared by pyrolysis of MCA at 600 °C, according to a previously described procedure [19].

Characterization

The characteristics of the synthesized composite were evaluated by X-ray powder diffraction, using a Bruker (Billerica, MA, USA) D8 Discover diffractometer (CuKα=1.5418 Å); and by attenuated total reflectance Fourier-transform infrared spectroscopy (ATR-FTIR) with an Agilent (Santa Clara, CA, USA) Cary 630 spectrophotometer.

The morphology of the samples was investigated by transmission electron microscopy (TEM) with a JEOL (Peabody, MA, USA) JEM–FS2200 HRP apparatus, equipped with an energy dispersion spectroscopy (EDS) probe.

UV-Vis spectra, both in reflectance and transmission modes, were obtained with an Agilent UV-Vis Cary 100.

The Brunauer-Emmett-Teller (BET) surface area and Barrett-Joyner-Halenda (BJH) methods were performed with a Micromeritics (Norcross, GA, USA) ASAP2020 adsorption isotherm equipment, with N_2 as the adsorbed gas and at a temperature of 77.350 K.

The analysis by X-ray photoelectron spectroscopy was performed using a Thermo Scientific (Waltham, MA, USA) K-Alpha ESCA instrument equipped with aluminum Kα monochromatized radiation at 1486.6 eV X-ray source. Due to the non-conductive nature of the samples (the presence of Ag, Fe and graphite in small amounts was not sufficient to make it conductive), it was necessary to use an electron flood gun to minimize surface charging. Neutralization of the surface charge was performed by using both a low energy flood gun (electrons in the range 0 to 14 eV) and a low energy Argon

ions gun. The XPS measurements were carried out using monochromatic Al-Kα radiation ($h\nu$=1486.6 eV). Photoelectrons were collected from a take-off angle of 90º relative to the sample surface. The measurement was done in a Constant Analyser Energy mode (CAE) with a 100 eV pass energy for survey spectra and 20 eV pass energy for high-resolution spectra. Charge referencing was done by setting the lower binding energy C 1s photo peak at 285.0 eV C1s hydrocarbon peak [20]. Surface elemental composition was determined using the standard Scofield photoemission cross sections.

Thermal gravimetric (TGA) and differential scanning calorimetry (DCS) analyses of the composite AgFeCN were carried out by means of a SETSYS Evolution 1750 Simultaneous TGA DSC Thermal Analyzer (Setaram Instrumentation, Caluire-et-Cuire, France), in both air and nitrogen, with a flow heating rate of 10 °C·min^{-1}.

Time of flight secondary ion mass spectrometry (TOF-SIMS) was used to check the presence of silver ions and other charged species in the composite. In order to identify ionic fragments that could allow to confirm the presence of certain species, the mass spectra of the samples were recorded on a TOF-SIMS IV instrument (IONTOF GmbH, Münster, Germany). The sample was bombarded with a pulsed Bismuth ion beam. The secondary ions generated were extracted with a 10 kV voltage and their time of flight from the sample to the detector was measured in a reflectron mass spectrometer.

For pristine g-C_3N_4 characterization, the interested reader is referred to previous reports [19,21,22].

Photocatalytic tests

To assess the ability of the new photocatalyst to carry out photo-reduction in competition with oxidative processes, crystal violet (CV^+; CAS No. 548-62-9, Sigma-Aldrich, ≥90% anhydrous basis) was used a redox indicator.

A solution of CV^+ (50 ppm) with tri-sodium citrate (tri-sodium citrate di-hydrate, CAS No. 6132-04-3; Sigma Aldrich, >99%) 0.39 M (given that citrate ion works as a hole scavenger, favors reduction and inhibits oxidation), with 8.6 g·L^{-1} of catalyst was monitored under solar light exposition (ca. 900 W·m^{-2}, T=29 °C [23]).

To control the different behavior of the catalysts, a complementary series of qualitative experiments was carried out with citric acid (anhydrous, CAS No. 77-92-9; Sigma Aldrich, ACS reagent >99%), which favors the photo-oxidation of CV^+ and inhibits the reduction mechanism.

Another series of quantitative experiments was carried out by irradiating the samples with a 55 W H1 Xenon-type lamp at a distance 10 cm from the cells (3.5 mL of solution) using H_2O_2 at a concentration of 0.24 wt% with 0.050 g of catalyst. The other components (e.g., CV^+) were used in the same amounts as in the experiment with tri-sodium citrate in order to compare the effect of catalyst type on the reaction mechanism towards either oxidation or reduction of crystal violet.

The concentration of CV^+ was monitored at 580 nm, normalized with respect to the initial value, while full spectra were recorded from 300 to 800 nm and taken at fixed intervals of time, as reported in the next section.

The conversion rate by unit of surface area was determined according to Eq. (1):

$$\text{Conversion rate} = \frac{C_{t1}-C_{t2}}{C_0(t_2-t_1)} \cdot \frac{1}{mA_s} \quad (1)$$

where C_{t1} and C_{t2} are the CV^+ concentrations at time t_1 and t_2 ($t_2>t_1$), respectively, C_0 is the initial CV^+ concentration, m is the catalyst mass (g) and is A_s the catalyst surface area (expressed in m^2·g^{-1}).

RESULTS AND DISCUSSION

Characterization of the AgFeCN composite

The infrared (IR) spectrum of the AgFeCN composite was compatible with that of carbon nitride. Neither β-Ag_2Se nor γ-Fe_2O_3 had any remarkable influence on the spectrum, which is reported in the Supplementary Information together with the spectrum of CV^+ in water solution (Figure S1). Information about the used graphite can be found a previous report [24]. An in-detail interpretation of the IR spectrum of g-C_3N_4 has already been reported in previous research reports by the same research group, and for sake of brevity is not further discussed [4,19,21].

The UV-Vis spectra are depicted in Figure 2. The AgFeCN sample exhibited a higher absorption in the region between 300 and 400 nm. The shoulder at around 400 nm can be attributed to the other compounds present in the AgFeCN composite. However, other bands below 400 nm are not appreciable, probably because they would be overwhelmed by the carbon nitride absorption. The optical bandgaps calculated by a Tauc plot [25] (reported in Figure S2) were 3.12 and 3.05 eV for CN and AgFeCN, respectively.

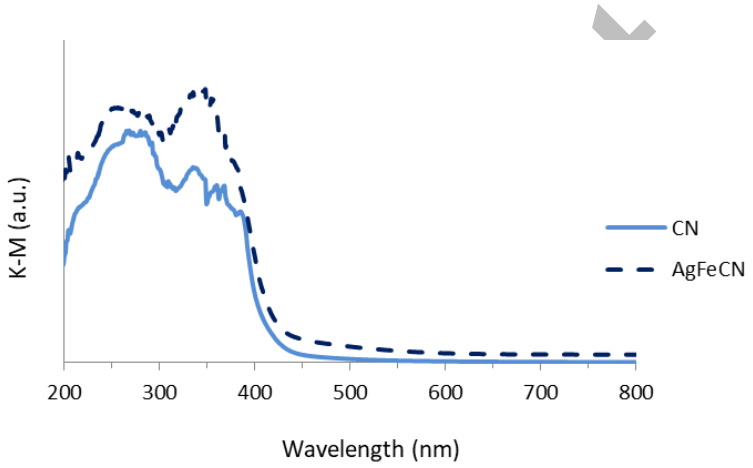

Figure 2. UV-Vis spectra of the AgFeCN composite and of pristine g-C_3N_4 (CN).

The X-ray diffraction patterns of AgFeCN and CN are shown in Figure 3. The sharp peak at 26.5° belongs to (002) reflection of graphite, while the peak at 27.2° and the shoulder at 27.8° can be attributed to (002) reflection of g-C_3N_4 [19,20]. The double signal can be due to distortions resulting from the presence of graphite. Ag_2Se exhibited several peaks at 30.9° (102), 33.5° (112), 34.8° (112) and 36.9° (121), and other smaller ones at 40.0° (031), 42.6° (113), 43.5° (201), and 45.2° (023) [12,26], while the other small peaks at 44.5° and 54.5° correspond to graphite. The peak at 35.6° (311) can be ascribed to maghemite phase of Fe_2O_3 (γ-Fe_2O_3) [14].

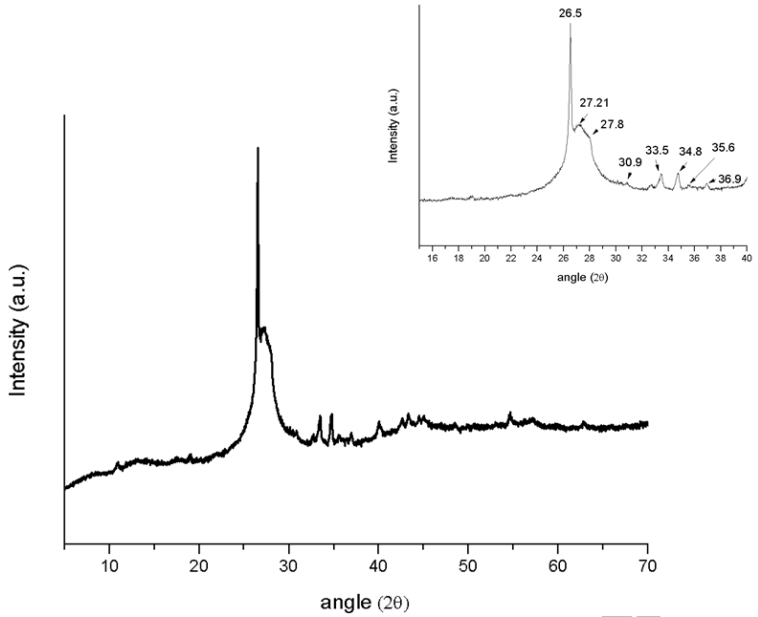

Figure 3. XRD pattern of AgFeCN composite. The inset shows the position of the main peaks in the region between 15° and 40°.

The BET [27] results showed that the surface areas were 74.91 and 4.38 $m^2 \cdot g^{-1}$ for CN and AgFeCN, respectively (i.e., the surface area of g-C_3N_4 was 17-fold that of the AgFeCN composite material). The pore surface areas obtained by BJH were 62.96 and 3.46 $m^2 \cdot g^{-1}$, and the average pore diameters were 35.08 and 65.22 nm for CN and AgFeCN, respectively. The adsorption and desorption curves are presented in Figure S3.

The TGA in air and in nitrogen of the AgFeCN composite (Figures S4 and S5) revealed that inorganic matter (oxides and selenides of Ag and Fe) accounted for ca. 9 wt%, while graphite was estimated to account for ca. 3.5 wt%. In the DSC curve (Figure 4), a sharp endotherm was observed at 719 °C (overlaid with the decomposition peak of g-C_3N_4), tentatively ascribed to the solid to liquid phase change of silver selenides [28,29]. The lower melting temperature with respect that reported in other works (880 °C) would be due to the nanometric size of the particles and embedding in the g-C_3N_4 composite.

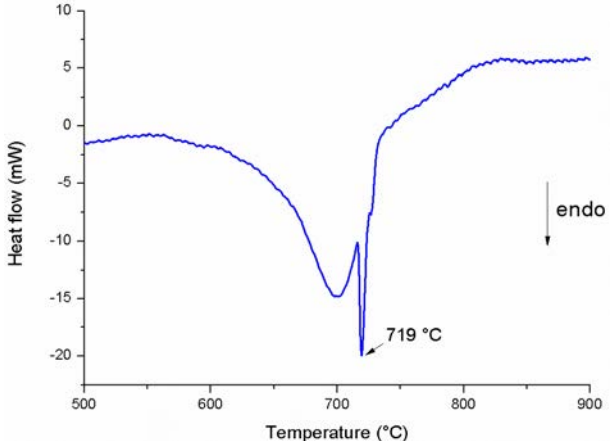

Figure 4. DSC curve of the AgFeCN composite in the 500-900 °C range.

The TEM investigation showed nanoparticles of iron oxide, graphite and silver selenide, all embedded in g-C_3N_4 (Figure 5). Silver selenide particles exhibited a

droplet shape attached onto the carbon nitride surface (they were detected by EDS probe), while iron oxide appeared as very tiny irregular particles. The crystallinity of graphite could be also appreciated through the parallel dense lines of (002) planes.

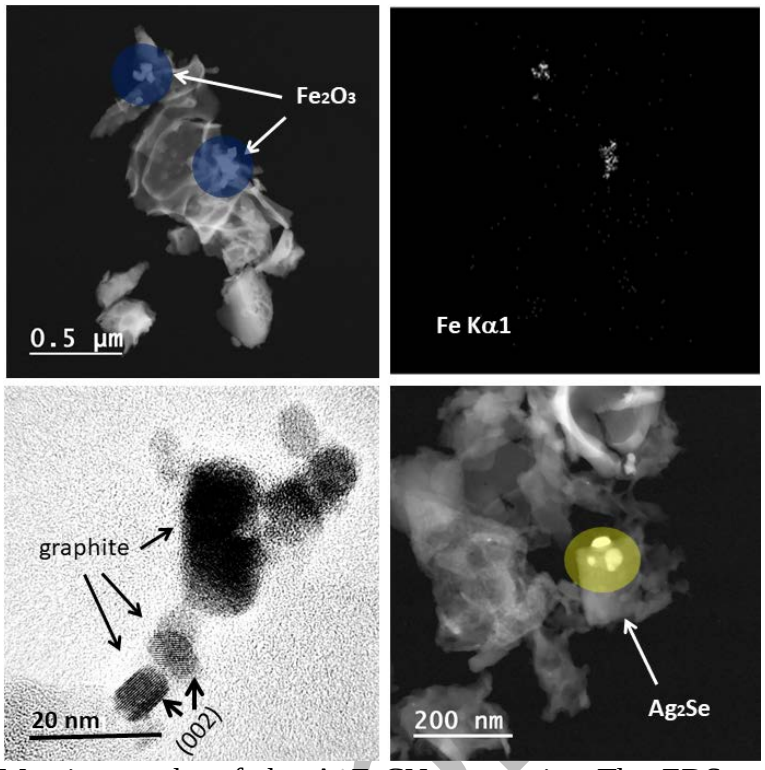

Figure 5. TEM micrographs of the AgFeCN composite. The EDS map of Fe K1a (upper right image) is shown with respect to the image on its left.

TOF-SIMS analysis revealed that Ag was spread over all the surface, with some concentrated clusters (Figure S6), and anions of CN, C_2N, CN_2, C_3N, C_3N_2, C_4N_3, C_3N_4 (typical of carbon nitride) were also detected among many other combinations.

XPS results showed C1s and N1s compatible with g-C_3N_4 and with the presence of graphite, as shown in Figures S7 and S8. Fe2p bands (shown in Figure S9), attributed to Fe^{2+} and Fe^{3+}, were compatible with γ-Fe_2O_3. The spectrum at low energies (Figure 6) indicated a valence band position of +3.1 eV with respect to the Fermi level, similar to the optical bandgap value, thus indicating that the exciton binding energy must be considerable, as expected from a polymeric carbon nitride (usually between 300 and 800 meV, depending on the material structure [30]).

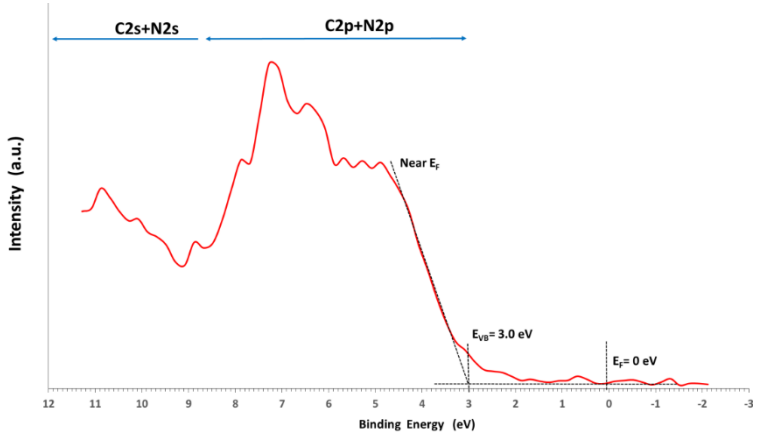

Figure 6. Valence band (VB) structure of AgFeCN composite as determined by XPS at low binding energies. E_F and E_{VB} stand for Fermi level and VB energy, respectively.

Photocatalytic activity

The reduction reaction of CV^+ is presented in Eq. (2),

$$CV^+ + H_2O \leftrightharpoons LCV + {}^1/_2\, O_2 + H^+ \quad (2)$$

This reduction can take place either by electron transfer directly on the active sites or mediated by H_2 obtained from direct water splitting by the photocatalyst, as shown in Figure 7. Both mechanisms would be favored by the presence of tri-sodium citrate, which –as noted above– works as a hole scavenger [31] and creates a basic environment (initial pH =9).

However, LCV is known to behave as an electron donor to semiconductors such as fullerenes (C_{60}) [32], i.e., it is able to transfer hydrogen and electrons to suitable semiconductors. In fact, it has already been studied for hydride transfer to reduce methylene blue in reactions activated by UV and visible light [33]. Therefore, it cannot be excluded that the reaction in Eq. (2) may also be mediated through a hydride transfer from CN, which is rich in hydrogen and energetic electrons, to CV^+.

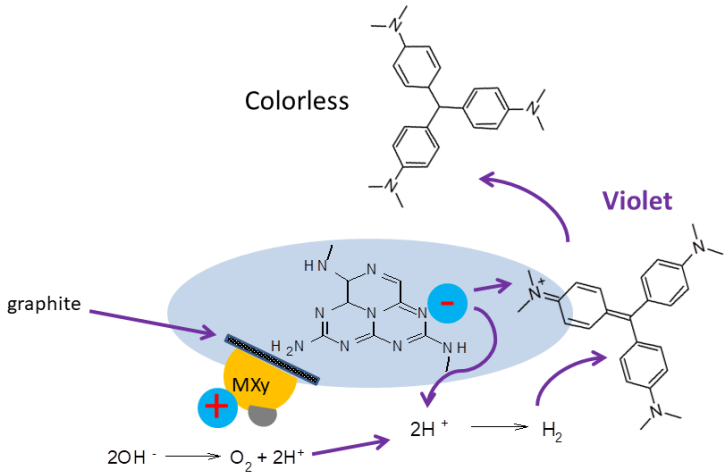

Figure 7. Sketch showing the possible reaction mechanisms involved in the reduction of crystal violet to leuco crystal violet. MX_y can be either Ag_2Se or Fe_2O_3.

The results of CV^+ photo-reduction tests under solar light irradiation, at approximately 900 $W \cdot m^{-2}$ in the presence of tri-sodium citrate, are summarized in Figure 8. The presence of Ag_2Se and Fe_2O_3 co-catalysts in the AgFeCN composite

made it much more active (about 20 times) than pristine g-C_3N_4 (CN). However, as noted above, the surface area of CN was *ca.* 17 times higher than that of AgFeCN, compensating for the low activity of CN.

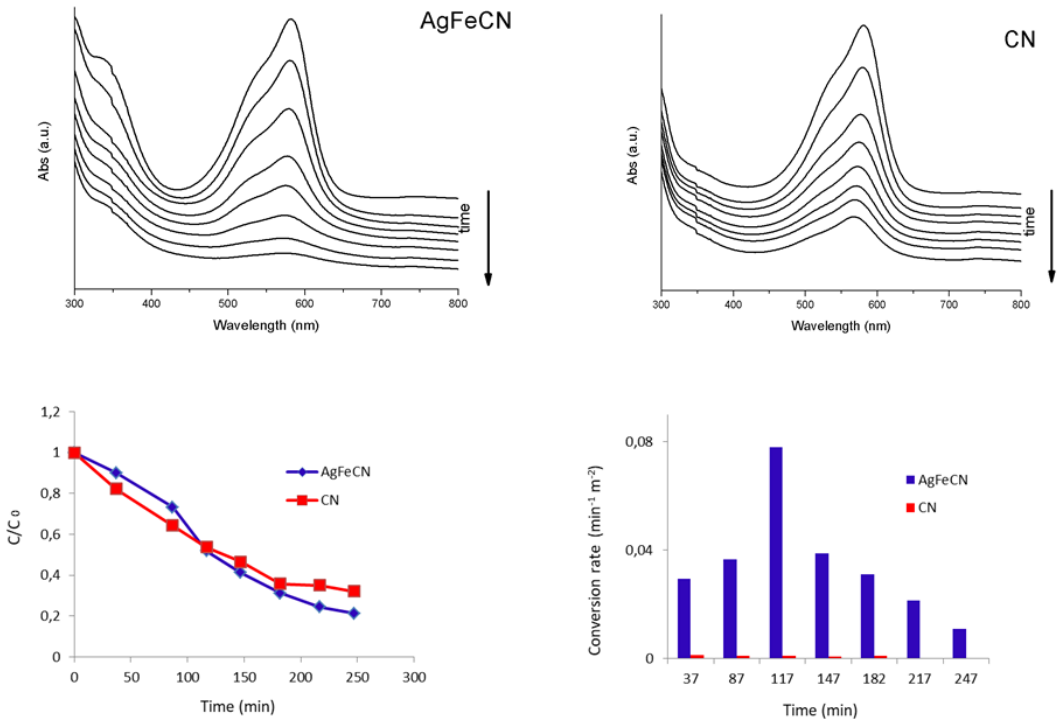

Figure 8. *Top*: UV-Vis spectra of the reduction of CV^+ using the AgFeCN composite (*left*) and pristine g-C_3N_4 (CN, *right*) as photocatalysts. *Bottom left*: evolution of CV^+ concentration (determined at 580 nm) as a function of time. *Bottom right*: conversion rate by unit of surface area for the AgFeCN composite and CN (in the graphic the second bar from left to right is referred to CN).

An enhanced performance of AgFeCN composite was also found in the oxidation of CV^+ in the presence of H_2O_2 (Figure 9), with conversion rates approximately 8 times higher than those of CN.

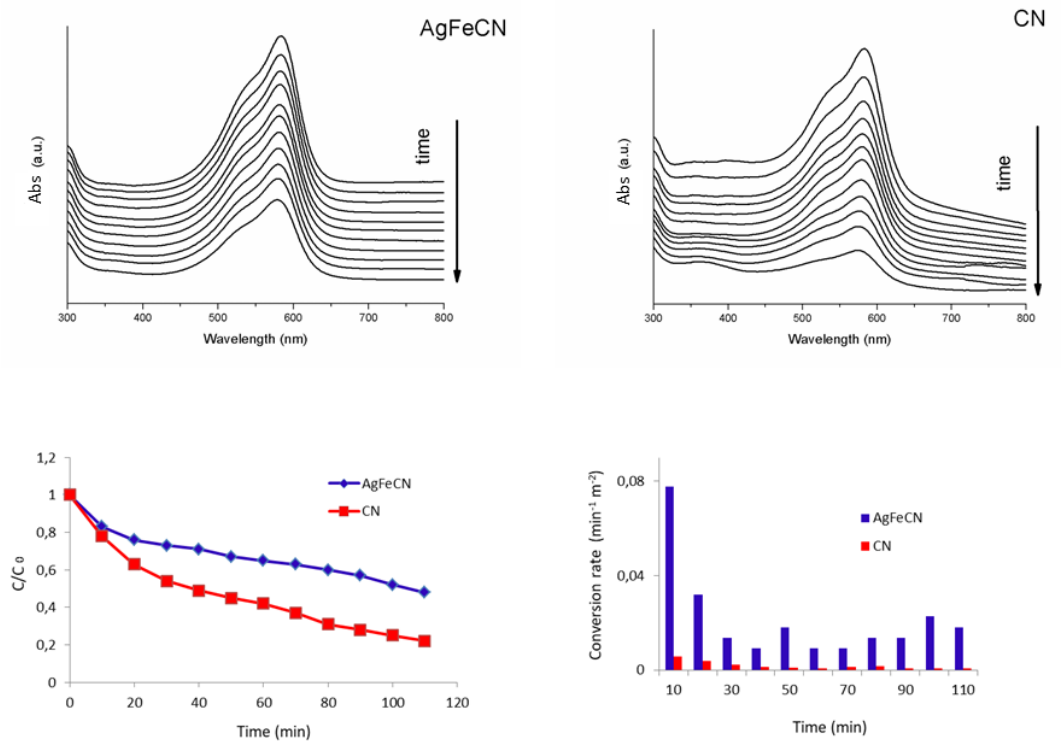

Figure 9. *Top*: UV-Vis spectra of the oxidation of CV^+ in the presence of H_2O_2 using the AgFeCN composite (*left*) and pristine g-C_3N_4 (CN, *right*) as photocatalysts. *Bottom left*: evolution of CV^+ concentration (determined at 580 nm) as a function of time. *Bottom right*: conversion rate by unit of surface area for the AgFeCN composite and CN (in the graphic the second bar from left to right is referred to CN).

The color changes of the photocatalytic tests are shown in Figure 10. Given that the reduction reaction shown in Eq. (2) is reversible by exposure to air oxidation (and light) and by acidification, it may be observed that the solutions that had previously been exposed to solar light irradiation for photocatalytic reduction, eventually recovered their original violet color.

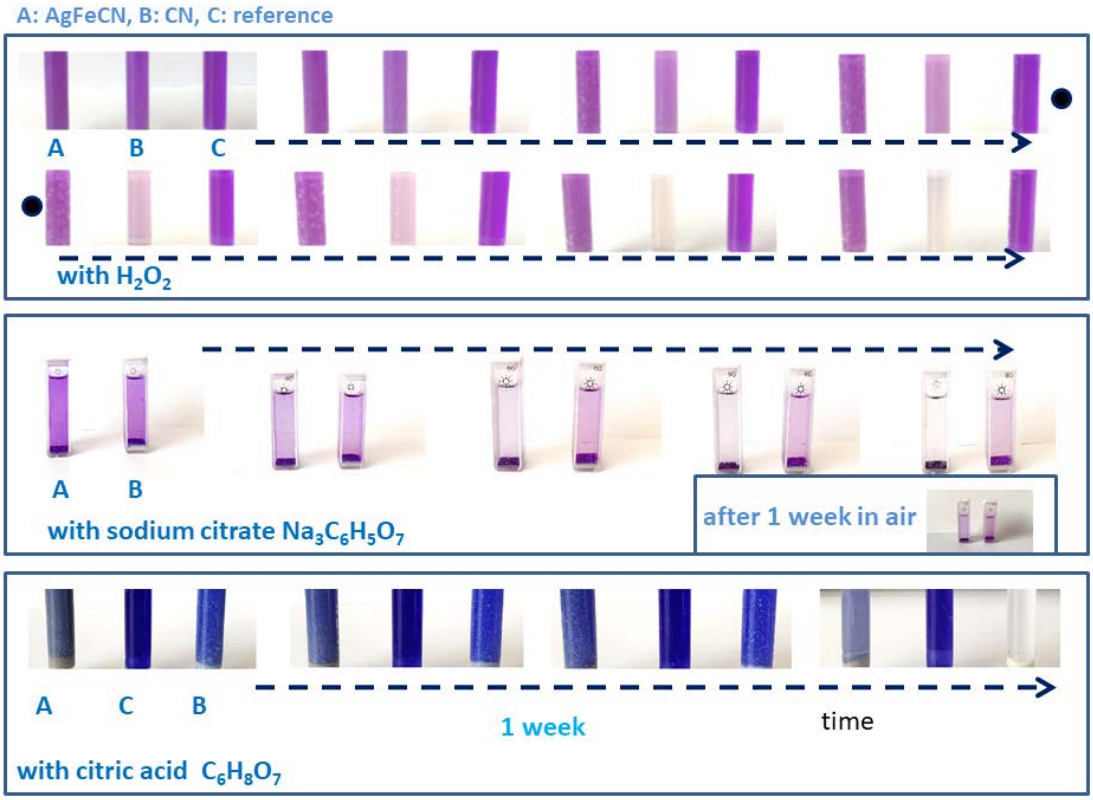

Figure 10. *Top*: color changes in the presence of H_2O_2 photo-oxidation, reduction test with sodium citrate, and qualitative test with citric acid as function of time. After one week exposure to air (following the reduction test), the color of CV^+ was partially recovered by oxidation (and acidification). The arrows indicate time direction. Oxidation and reduction test times were already shown in Fig.9.

Figure 10 also shows the results from a visual test conducted with citric acid, which should inhibit reduction. It may be observed that the solution with CN was fully discolored in a week, while that of AgFeCN composite was not. This finding would further support that the Z scheme in AgFeCN was more effective towards CV^+ reduction than that found CN.

It is worth noting that both the reduction (with tri-sodium citrate) and the oxidation tests (with hydrogen peroxide) were repeated after washing of the catalyst with deionized water, leading to similar results after 5 cycles (with a decrease in conversion rate <5%), pointing to a good reusability of the composite. Therefore, with a view to the applicability of the composite, at this point the main limitation detected would concern its low surface area. Thus, alternative synthesis methods need to be assayed. For instance, by synthesizing Ag_2Se and Fe_2O_3 separately and then mixing them with high-surface area mesoporous g-C_3N_4 (produced by solvothermal, co-condensation, hydrothermal, microemulsion or microfluidic synthesis methods [34]), followed by annealing. Further work in this line of research is underway.

CONCLUSIONS

The physico-chemical properties of a novel composite (AgFeCN), consisting of three semiconductors (β-Ag_2Se, γ-Fe_2O_3, g-C_3N_4) and graphite as a conductor, were studied by XRD, FTIR, UV-Vis, TEM, XPS, TGA, DSC and TOF-SIMS. As a first step in the

study of the applicability of this Z scheme, the ability of the composite material to act as a photoreductant/photooxidant was assessed using crystal violet redox indicator. In the presence of tri-sodium citrate and under solar light irradiation, the conversion rates per unit of surface area towards reduction for the AgFeCN composite were ~20 times higher than those of pristine g-C_3N_4. In the photo-oxidation experiments, upon irradiation with a Xe lamp and in the presence of H_2O_2, the AgFeCN composite was ~8 times more active than pristine g-C_3N_4. This fact indicated that the material is more inclined to photoreduction. Although its performance is still limited by its low surface area, pointing to the need for developing alternative synthesis methods, the chosen Z-scheme may hold promise for obtaining either hydrogen or hydrogenated compounds. Moreover, the photoreduction of crystal violet to leuco crystal violet can be used as a simple procedure to select photocatalysts to be effective photoreductants towards hydrogen production.

Acknowledgments
The authors are very grateful to the Scientific and Technological Research Assistance Centre (CACTI), University of Vigo, where some of the characterizations were performed (TEM, XPS and TOF-SIMS).

REFERENCES

[1] J. Liebig, Uber einige Stickstoff - Verbindungen, Annalen der Pharmacie, 10 (1834) 1-47.
[2] L. Pauling, J.H. Sturdivant, The structure of cyameluric acid, hydromelonic acid and related substances, Proc. Natl. Acad. Sci., 23 (1937) 615-620.
[3] P. Chamorro-Posada, P. Martín-Ramos, F.M. Sánchez-Arévalo, R.C. Dante, Molecular dynamics simulations of nanosheets of polymeric carbon nitride and comparison with experimental observations, Fullerenes, Nanotubes, Carbon Nanostruct., 26 (2018) 137-144.
[4] R.C. Dante, F.M. Sánchez-Arévalo, P. Chamorro-Posada, J. Vázquez-Cabo, L. Huerta, L. Lartundo-Rojas, J. Santoyo-Salazar, O. Solorza-Feria, A. Diaz-Barrios, T. Zoltan, F. Vargas, T. Valenzuela, F. Muñoz-Bisesti, F.J. Quiroz-Chávez, Synthesis and characterization of Cu-doped polymeric carbon nitride, Fullerenes, Nanotubes, Carbon Nanostruct., 24 (2015) 171-180.
[5] A. Naseri, M. Samadi, A. Pourjavadi, A.Z. Moshfegh, S. Ramakrishna, Graphitic carbon nitride (g-C_3N_4)-based photocatalysts for solar hydrogen generation: recent advances and future development directions, J. Mater. Chem. A, 5 (2017) 23406-23433.
[6] R. Zhang, Y. Wang, Z. Zhang, J. Cao, Highly sensitive acetone gas sensor based on g-C_3N_4 decorated $MgFe_2O_4$ porous microspheres composites, Sensors, 18 (2018).
[7] T. Lin, L. Zhong, J. Wang, L. Guo, H. Wu, Q. Guo, F. Fu, G. Chen, Graphite-like carbon nitrides as peroxidase mimetics and their applications to glucose detection, Biosens. Bioelectron., 59 (2014) 89-93.
[8] T.R. Chetia, M.S. Ansari, M. Qureshi, Graphitic carbon nitride as a photovoltaic booster in quantum dot sensitized solar cells: a synergistic approach for enhanced charge separation and injection, J. Mater. Chem. A, 4 (2016) 5528-5541.
[9] J.R. Bolton, S.J. Strickler, J.S. Connolly, Limiting and realizable efficiencies of solar photolysis of water, Nature, 316 (1985) 495-500.

[10] B. Dembinska, K. Brzozowska, A. Szwed, K. Miecznikowski, E. Negro, V. Di Noto, P.J. Kulesza, Electrocatalytic oxygen reduction in alkaline medium at graphene-supported silver-iron carbon nitride sites generated during thermal decomposition of silver hexacyanoferrate, Electrocatalysis, 10 (2018) 112-124.
[11] J. Feng, Q. Shi, Y. Li, J. Huang, R. Li, X. Shu, W. Li, X. Xie, Pyrolysis preparation of poly-γ-glutamic acid derived amorphous carbon nitride for supporting Ag and γ-Fe_2O_3 nanocomposites with catalytic and antibacterial activity, Materials Science and Engineering: C, 101 (2019) 138-147.
[12] D.W. Ayele, A facile one-pot synthesis and characterization of Ag_2Se nanoparticles at low temperature, Egyptian Journal of Basic and Applied Sciences, 3 (2019) 149-154.
[13] B. Pejova, M. Najdoski, I. Grozdanov, S.K. Dey, Chemical bath deposition of nanocrystalline (111) textured Ag_2Se thin films, Mater. Lett., 43 (2000) 269-273.
[14] R.A. Bepari, P. Bharali, B.K. Das, Controlled synthesis of α- and γ-Fe_2O_3 nanoparticles via thermolysis of PVA gels and studies on α-Fe_2O_3 catalyzed styrene epoxidation, Journal of Saudi Chemical Society, 21 (2017) S170-S178.
[15] R.C. Dante, Water photolysis by carbon nitride, Int. J. Hydrogen Energy, 44 (2019) 21030-21036.
[16] M. Mousavi, A. Habibi-Yangjeh, Magnetically separable ternary g-C_3N_4/Fe_3O_4/BiOI nanocomposites: Novel visible-light-driven photocatalysts based on graphitic carbon nitride, J. Colloid Interface Sci., 465 (2016) 83-92.
[17] Y. Xu, M.A.A. Schoonen, The absolute energy positions of conduction and valence bands of selected semiconducting minerals, Am. Mineral., 85 (2000) 543-556.
[18] M.M. Islam, K. Ueno, H. Misawa, Redox cycling effect on the surface-enhanced Raman scattering signal of crystal violet molecules at nanostructured interdigitated array electrodes, Anal. Sci., 26 (2010) 19-24.
[19] R.C. Dante, P. Martín-Ramos, F.M. Sánchez-Arévalo, L. Huerta, M. Bizarro, L.M. Navas-Gracia, J. Martín-Gil, Synthesis of crumpled nanosheets of polymeric carbon nitride from melamine cyanurate, J. Solid State Chem., 201 (2013) 153-163.
[20] D. Briggs, M.P. Seah, Practical surface analysis, Auger and X-ray photoelectron spectroscopy, 2nd ed., John Wiley & Sons Ltd, Chichester; New York, 1990.
[21] R.C. Dante, P. Martín-Ramos, L.M. Navas-Gracia, F.M. Sánchez-Arévalo, J. Martín-Gil, Polymeric carbon nitride nanosheets, J. Macromol. Sci., Phys., 52 (2013) 623-631.
[22] R.C. Dante, F.M. Sánchez-Arévalo, P. Chamorro-Posada, J. Vázquez-Cabo, L. Huerta, L. Lartundo-Rojas, J. Santoyo-Salazar, O. Solorza-Feria, Supramolecular intermediates in the synthesis of polymeric carbon nitride from melamine cyanurate, J. Solid State Chem., 226 (2015) 170-178.
[23] Dipartimento di Fisica - Università degli Studi di Torino, Dati del giorno martedì 16/07/2019, Stazione Meteorologica di Fisica dell'Atmosfera, Università degli Studi di Torino, Torino, Italy, 2019.
[24] P. Chamorro-Posada, J. Vázquez-Cabo, Ó. Rubiños-López, J. Martín-Gil, S. Hernández-Navarro, P. Martín-Ramos, F.M. Sánchez-Arévalo, A.V. Tamashausky, C. Merino-Sánchez, R.C. Dante, THz TDS study of several sp2 carbon materials: Graphite, needle coke and graphene oxides, Carbon, 98 (2016) 484-490.

[25] J. Tauc, R. Grigorovici, A. Vancu, Optical properties and electronic structure of amorphous germanium, Physica Status Solidi B: Basic Solid State Physics, 15 (1966) 627-637.
[26] S.P. Anthony, Synthesis of Ag_2S and Ag_2Se nanoparticles in self assembled block copolymer micelles and nano-arrays fabrication, Mater. Lett., 63 (2009) 773-776.
[27] M. Thommes, K. Kaneko, A.V. Neimark, J.P. Olivier, F. Rodriguez-Reinoso, J. Rouquerol, K.S.W. Sing, Physisorption of gases, with special reference to the evaluation of surface area and pore size distribution (IUPAC Technical Report), Pure Appl. Chem., 87 (2015) 1051.
[28] O. Madelung, U. Rössler, M. Schulz, Silver selenide (Ag_2Se) optical and further properties, in: O. Madelung, U. Rössler, M. Schulz (Eds.) Non-Tetrahedrally Bonded Elements and Binary Compounds I, Springer-Verlag, Berlin Heidelberg, 1998, pp. 1-7.
[29] A.J.E. Rettie, C.D. Malliakas, A.S. Botana, J.M. Hodges, F. Han, R. Huang, D.Y. Chung, M.G. Kanatzidis, Ag_2Se to KAg_3Se_2: Suppressing order–disorder transitions via reduced dimensionality, J. Am. Chem. Soc., 140 (2018) 9193-9202.
[30] S. Melissen, T. Le Bahers, S.N. Steinmann, P. Sautet, Relationship between carbon nitride structure and exciton binding energies: A DFT perspective, The Journal of Physical Chemistry C, 119 (2015) 25188-25196.
[31] M. Liu, L. Luo, F. Dong, H. Wei, X. Nie,W. Zhang, W. Hu, C. Ding, P. Wang, Characteristics and mechanism of uranium photocatalytic removal enhanced by chelating hole scavenger citric acid in a TiO2 suspension system, Journal of Radioanalytical and Nuclear Chemistry, 319 (2019) 147-158.
[32] F. Li, A. Werner, M. Pfeiffer, K. Leo, X. Liu, Leuco crystal violet as a dopant for n-doping of organic thin films of fullerene C_{60}, The Journal of Physical Chemistry B, 108 (2004) 17076-17082.
[33] Y. Liu, S. Yamamoto, Y. Sueishi, Photoinduced hydride transfer reaction between methylene blue and leuco crystal violet, J. Photochem. Photobiol. A: Chem., 143 (2001) 153-159.
[34] O. Alduhaish, M. Ubaidullah, A.M. Al-Enizi, N. Alhokbany, S.M. Alshehri, J. Ahmed, Facile synthesis of mesoporous α-Fe_2O_3@g-C_3N_4-NCs for efficient bifunctional electro-catalytic activity (OER/ORR), Sci. Rep., 9 (2019).